2002MNRAS.335..871H

Mon. Not. R. Astron. Soc. **335,** 871–882 (2002)

Breaking the 'redshift deadlock' – I. Constraining the star formation history of galaxies with submillimetre photometric redshifts

D. H. Hughes,[1★] I. Aretxaga,[1] E. L. Chapin,[1] E. Gaztañaga,[1,2] J. S. Dunlop,[3] M. J. Devlin,[4] M. Halpern,[5] J. Gundersen,[6] J. Klein,[4] C. B. Netterfield,[7] L. Olmi,[8] D. Scott[9] and G. Tucker[10]

[1]*Instituto Nacional de Astrofísica, Óptica y Electrónica (INAOE), Aptdo. Postal 51 y 216, Puebla, Mexico*
[2]*Institut d'Estudis Espacials de Catalunya – IEEC/CSIC Gran Capitan 2-4, 08034 Barcelona, Spain*
[3]*Institute for Astronomy, Univ. Edinburgh, Blackford Hill, Edinburgh EH9 3HJ*
[4]*Department of Physics & Astronomy, Univ. of Pennslyvania, 209 South 33rd St., Philadelphia, PA 19104-6396, USA*
[5]*Department of Physics & Astronomy, Univ. of British Columbia, 6224 Agricultural Road, Vancouver, BC V6T 1Z1, Canada*
[6]*Department of Physics, Univ. of Miami, 1320 Campo Sano Drive, Coral Gables, FL 33416, USA*
[7]*Department of Astronomy, Univ. of Toronto, 60 St George St., Toronto, Ontario, MSS 1A1, Canada*
[8]*Physics Department, University of Puerto Rico, PO Box 23343, University Station San Juan, PR 00931-3343, Puerto Rico*
[9]*Department of Physics & Astronomy, Univ. of British Columbia, 2219 Main Mall, Vancouver, BC V6T 1Z4, Canada*
[10]*Department of Physics, Box 1843, Brown Univ., Providence, RI 02912-1843, USA*

Accepted 2002 May 8. Received 2002 April 28; in original form 2001 December 10

ABSTRACT

Future extragalactic submillimetre and millimetre surveys have the potential to provide a sensitive census of the level of obscured star formation in galaxies at all redshifts. While in general there is good agreement between the source counts from existing Submillimetre Common User Bolometer Array (SCUBA; 850-μm) and Max Planck Millimetre Bolometer Array (MAMBO; 1.25-mm) surveys of different depths and areas, it remains difficult to determine the redshift distribution and bolometric luminosities of the submillimetre and millimetre galaxy population. This is principally due to the ambiguity in identifying an individual submillimetre source with its optical, IR or radio counterpart which, in turn, prevents a confident measurement of the spectroscopic redshift. Additionally, the lack of data measuring the rest-frame FIR spectral peak of the submillimetre galaxies gives rise to poor constraints on their rest-frame FIR luminosities and star formation rates. In this paper we describe Monte Carlo simulations of ground-based, balloon-borne and satellite submillimetre surveys that demonstrate how the rest-frame FIR–submillimetre spectral energy distributions (250–850 μm) can be used to derive photometric redshifts with an rms accuracy of ±0.4 over the range $0 < z < 6$. This opportunity to break the redshift deadlock will provide an estimate of the global star formation history for luminous optically obscured galaxies ($L_{\rm FIR} > 3 \times 10^{12}$ L$_\odot$) with an accuracy of ∼20 per cent.

Key words: surveys – galaxies: evolution – galaxies: formation – galaxies: high-redshift – cosmology: observations – submillimetre.

1 INTRODUCTION

The star formation history of the high-z starburst galaxy population can be determined from an accurate measurement of the integral submillimetre (sub-mm) and millimetre (mm) source counts, and the luminosity and redshift distributions of sub-mm and mm-selected galaxies. The contribution of these sources to the total FIR–mm background, measured by COBE (Puget et al. 1996; Hauser et al. 1998; Fixsen et al. 1998), places an additional strong constraint on the acceptable evolutionary models. It is now generally believed that the luminosity density, owing to star formation activity in galaxies, is roughly constant between $z \sim 1$–4. A series of ground-based 850-μm surveys (Smail, Ivison & Blain 1997; Hughes et al. 1998; Barger et al. 1998; Eales et al. 1999, 2000; Scott et al. 2002; Fox et al. 2002; Borys et al. 2001), undertaken with the SCUBA camera (Holland et al. 1999) on the 15-m James Clerk Maxwell Telescope (JCMT) and 1.25-mm surveys (Bertoldi et al. 2000) using the MAMBO camera (Kreysa et al. 1998) on the 30-m Institut de Radioastronomie Millimetrique (IRAM) telescope have contributed significantly to this understanding. Prior to the first SCUBA results, the optical surveys suggested (contrastingly) that the density of star formation declined by a factor of ∼5 over the same redshift range (Steidel et al. 1996;

★ E-mail: dhughes@inaoep.mx

© 2002 RAS

© Royal Astronomical Society • Provided by the NASA Astrophysics Data System

2002MNRAS.335..871H

Madau et al. 1996). This discrepancy has highlighted the importance of including a correction for dust extinction in the optical–UV estimates of star formation rates. Nevertheless, the contribution of optically selected starburst galaxies to the sub-mm background still remains uncertain (Chapman et al. 2000; Peacock et al. 2000). Hereafter, for the sake of brevity, sub-mm and mm wavelengths will be referred to as sub-mm unless explicitly stated otherwise, and a sub-mm galaxy is considered to be an optically obscured starburst galaxy detected in a blank-field SCUBA or MAMBO survey.

One important caveat to this opening statement is the fact that we actually have no accurate information on the redshift distribution of the sub-mm galaxy population. There are >100 galaxies identified in 850-μm surveys at a level >2 mJy. The lack of confident optical, or IR identifications (e.g. Hughes et al. 1998; Richards 1999), and thus precise redshifts for the sub-mm galaxies, was a source for the early scepticism of the claims that there existed no evidence for a strong decline in density of star formation at $z > 2$.

The use of the radio–sub-mm (850 μm/1.4 GHz) spectral index has gained popularity as a valuable diagnostic of redshift (Hughes et al. 1998; Carilli & Yun 1999, 2000; Smail et al. 2000; Barger, Cowie & Richards 2000; Dunne, Clements & Eales 2000). The radio follow-up of SCUBA surveys, and more recently 1.25-mm MAMBO surveys (Bertoldi et al. 2000) with the Very Large Array (VLA) at 1.4 GHz has become the commonly accepted method to measure the redshift distribution of sub-mm galaxies. However this technique requires extremely sensitive observations if radio counterparts are to be detected. For example, in order that a radio survey detects >90 per cent of bright sub-mm galaxies ($S_{850\,\mu\mathrm{m}} > 8$ mJy) at $z > 1.5$, then a $3\sigma \leqslant 7$ μJy survey must be conducted at 1.4 GHz (Aretxaga et al. 2002). Unfortunately the necessity of such an ultra-deep radio survey prohibits this technique from being applied to the wider-area (∼1–10 deg^2) sub-mm surveys that will be conducted in the next few years (Section 2) without an excessive commitment of radio telescope time (e.g. 400–4000 h per survey). An alternative, and, we argue, a more reliable method exists: namely the use of sub-mm–FIR photometric redshifts, provided that one can obtain experimental data with sufficient signal-to-noise ratio (S/N) and absolute calibration accuracy.

Although the possibility of conducting cosmological surveys at sub-mm and mm wavelengths has been realized in the last few years with the development and successful commissioning of sensitive bolometer arrays, the existing 850-μm SCUBA and 1.25-mm MAMBO surveys are limited in their ability to constrain the evolutionary models of the sub-mm galaxy population. The practical reasons for these limitations have been described elsewhere (Hughes 2000) and can be summarized as follows: restricted wavelength coverage (enforced by the limited number of FIR–mm atmospheric windows available to ground-based observatories); low spatial resolution (resulting in both a high extragalactic confusion limit and poor positional accuracy); restricted field-of-view with the current sub-mm and mm bolometer arrays (typically 5 arcmin^2); and low system sensitivity (a combination of instrument noise, size of telescope aperture and telescope surface accuracy, sky transmission and sky noise) which restrict even the widest and shallowest sub-mm surveys to areas <0.1 deg^2 (Scott et al. 2002; Fox et al. 2002). In the effort to obtain these wide-area shallow surveys, the current sub-mm and mm observations are necessarily only sensitive to the most luminous star-forming galaxies ($L_{\mathrm{FIR}} > 10^{12}$ $L_\odot$, or SFR > 100 $M_\odot$ yr^{-1}) assuming the population is dominated by galaxies at redshifts >1.

The discrepancy shown in Fig. 1 between the bright-end source counts in the 850-μm SCUBA and 1.25-mm MAMBO surveys (Eales et al. 2000; Bertoldi et al. 2000; Scott et al. 2002; Borys et al. 2002), and a visual inspection of their reconstructed maps, suggests that the clustering of sub-mm galaxies may be influencing the statistics (Gaztañaga & Hughes 2001). Taken at face value, the steepening of the 850-μm counts for sources >10 mJy can be interpreted as evidence for an under-density of galaxies in the survey

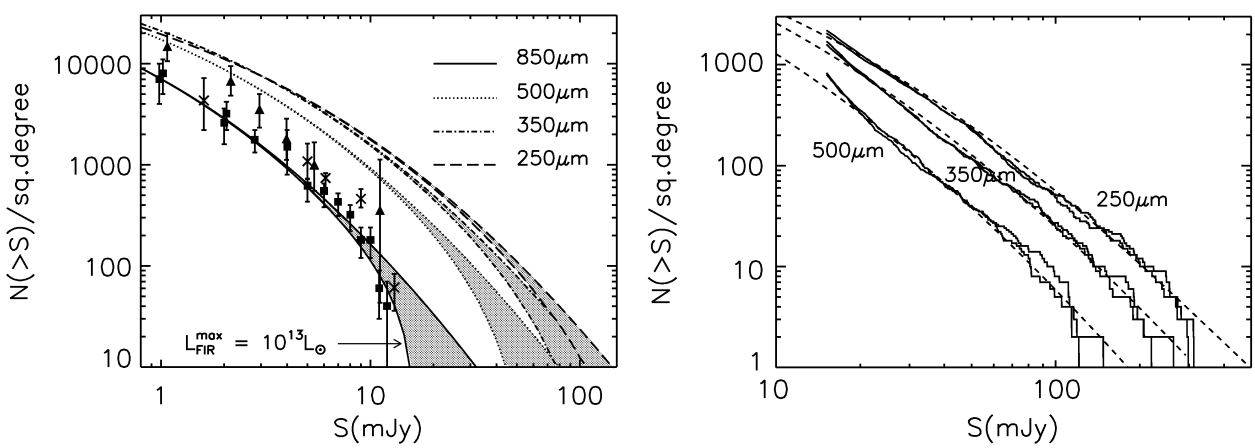

Figure 1. Integrated source counts at sub-mm wavelengths for a model in which the IRAS 60-μm luminosity function is evolved as $(1+z)^{3.2}$ up to $z = 2$, and maintained constant (with no further evolution) for $2 < z < 6$. The SED of Arp220 is adopted to represent the whole galaxy population. Left panel: the curves represent the predicted source counts at 850, 500, 350 and 250 μm. The measured source counts from SCUBA surveys at 850 μm (Scott et al. 2002, and references therein) are shown as filled squares. Additional 850-μm source counts from Borys et al. (2001) are shown as solid triangles. The flux-densities of the MAMBO 1.25-mm source counts are scaled upwards by a factor of 2.25 to represent the equivalent measurements at 850 μm, assuming the MAMBO sources lie at redshifts $0 < z < 6$, and are shown as crosses (Bertoldi et al. 2000). The models also show the effect of a high-luminosity cut-off (at $L_{\mathrm{FIR}} > 10^{13}$ $L_\odot$) in the sub-mm population. The shaded areas illustrate the regions of parameter space that need to be searched with future experiments to improve our understanding of the evolution of the luminous high-z sub-mm galaxies. Right panel: Integrated source counts for extragalactic BLAST surveys at 250, 350 and 500 μm. The dashed-lines show the same evolutionary model described for the left-panel. The histograms illustrate the extracted source counts at each wavelength from two different Monte Carlo simulations of 1 deg^2 surveys that use a library of 13 SEDs. These simulations explore evolutionary models with small differences in the strength of evolution and the redshift distribution of sources. The details of the Monte Carlo simulations are summarized in Section 2.2.

© Royal Astronomical Society • Provided by the NASA Astrophysics Data System

2002MNRAS.335..871H

field providing those particular data (owing to cosmic variance), or perhaps a high-luminosity cut-off in the luminosity function for galaxies $>10^{13}$ $L_\odot$ (Fig. 1). A plausible alternative explanation is simply the fact that, with so few bright sources detected (5–10 galaxies in 0.1 deg^2), the counts in this regime are extremely sensitive to differences between the spectral energy distributions (SEDs) of the most luminous sub-mm galaxies. Sensitive, wider-area ($\geqslant$1 deg^2), rest-frame FIR surveys with accurate redshift information (similar to those discussed in this paper) can distinguish between these possible alternatives.

1.1 Ambiguities in the counterparts of sub-mm galaxies

The current 850-μm SCUBA and 1.25-mm MAMBO surveys are struggling to identify the sub-mm sources with their optical, IR and radio counterparts. Positional errors of ∼2–3 arcsec are associated with the brightest sub-mm sources ($S_{850\,\mu\mathrm{m}} > 8$ mJy) which, with some exceptions, are detected in the widest, shallowest SCUBA surveys (Scott et al. 2002; Eales et al. 2000). These errors can be improved with follow-up mm-interferometric observations (Frayer et al. 1998; Gear et al. 2000; Lutz et al. 2001). However ambiguous optical identifications still remain, even with $\leqslant$2 arcsec resolution and subarcsec positional errors (e.g. Downes et al. 1999). It should be no surprise that sub-mm selected galaxies, including those with mm-interferometric detections, do not always have optical counterparts, since high-z galaxies observed in the earliest stages of formation may be heavily obscured by dust. Indeed, this is the most compelling reason for conducting the sub-mm surveys in the first instance. Searches for counterparts at longer IR wavelengths have proven to be more successful (Smail et al. 1999; Frayer et al. 2000; Gear et al. 2000; Lutz et al. 2001), and have shown earlier identifications of lower-z bright optical galaxies to be the incorrect counterpart to the sub-mm galaxies (Smail et al. 1999; Frayer et al. 2000). The natural consequence of these ambiguous and potential misidentifications is an inaccurate determination of redshift distribution, luminosities and star formation history of high-z galaxies.

1.2 Uncertainties in the SEDs and redshifts of sub-mm galaxies

Despite the diversity in the properties of sub-mm galaxies (Ivison et al. 2000), efforts have been made to place them in the context of an evolutionary model of galaxy formation. The current estimate of the redshift distribution of sub-mm galaxies is based on simple comparisons of their IR–radio SEDs with those of redshifted template SEDs, drawn from local starburst galaxies and radio-quiet active galactic nuclei (AGN) (Hughes et al. 1998; Smail et al. 1999; Lilly et al. 1999; Carilli & Yun 1999; Barger et al. 2000; Carilli & Yun 2000; Smail et al. 2000; Bertoldi et al. 2000; Dunne et al. 2000; Dunlop 2001; Smail et al. 2002; Chapman et al. 2002). The consensus is that the population of sub-mm galaxies is distributed between redshifts $z = 1$–4, with a median $z = 2$–3. The details of this distribution are still unknown, and it is common to describe the redshifts of individual galaxies as '*in the range of . . . . , with a best guess of . . . . .*'.

This raises an obvious question: *What classes of local galaxies offer the most useful analogues of the high-z sub-mm population?* In order to address this we must measure the full rest-frame X-ray to radio SEDs of individual high-z sub-mm galaxies, measure the dispersion in the shapes of their SEDs and their range of luminosities (which may depend on redshift), and thus determine the accuracy with which the SEDs of high-z sub-mm galaxies can be characterized by a limited number of local template galaxies. In practise, the observed SEDs of high-z sub-mm galaxies are restricted to a few detections and limits at 850 and 450 μm and 1.4 GHz, with occasional mm interferometric observations and a K-band identification. No data exist at rest-frame FIR wavelengths with sufficient sensitivity to place additional useful constraints on redshifts.

As mentioned previously, optical and IR follow-up observations of those few SCUBA sources for which unambiguous identifications exist have revealed that the sub-mm counterparts are often optically obscured, extremely red objects (EROs) with $I - K > 6$ (Smail et al. 1999; Gear et al. 2000; Lutz et al. 2001), although in a few cases the sub-mm counterparts are blue galaxies, with a weak AGN (e.g. SMM02399–0136, Ivison et al. 1999). Also the suggestion that SCUBA galaxies are forming stars at a very high rate ($>$100 $M_\odot$ yr^{-1}) implies that local dusty ultraluminous infrared galaxies (ULIRGs) may also be suitable analogues of high-z sub-mm sources. Unfortunately the SEDs of this local class of luminous star-forming galaxies vary significantly with increasing FIR luminosity (Sanders & Mirabel 1996). Furthermore, there are few starburst galaxies at $z > 1$ for which complete IR–radio SEDs exist.

These initial SCUBA and MAMBO observations have demonstrated the necessity for larger-area surveys, and also shorter-wavelength (250–500 μm) sub-mm observations. Although new (and future) ground-based facilities (e.g. 100-m Green Bank Telescope, 50-m Large Millimetre Telescope, Submillimetre Array, Combined Array for Research in Millimeter Astronomy) will offer partial solutions to some of these problems over the next 6 yr, there will still remain ambiguity in the optical, IR and radio identifications of sub-mm galaxies. The consequence is a lack of precision in the redshift distribution and rest-frame FIR luminosities, and thus an inaccurate constraint on the star formation history of the entire sub-mm population.

Once it begins operation beyond 2008, ALMA will undoubtedly solve many of these difficulties with its powerful combination of receivers operating between 350 μm and 3 mm, and high (sub-arcsec) spatial resolution. The expected launch of the *Herschel* satellite in 2008 will also bring the chance to map large areas of the extragalactic sky at 250–500 μm with high sensitivity. However, in late 2003 onwards, a series of long-duration (∼15 d) sub-orbital balloon flights will be undertaken by the Balloon-borne Large-Aperture Submillimetre Telescope (BLAST) (Devlin et al. 2001). BLAST has a 2-m primary aperture, and is equipped with large-format bolometer cameras operating at 250, 350 and 500 μm which are prototypes of the Spectral and Photometric Imaging Receiver (SPIRE) focal-plane cameras for the *Herschel* satellite. BLAST will conduct sub-mm surveys over ∼0.5–40 deg^2 (Table 1), and will provide rest-frame FIR–sub-mm data for $>$5000 galaxies, with a point-source sensitivity 3 times greater than is available from even the largest ground-based sub-mm telescopes.

In this paper (Paper I) we describe Monte Carlo simulations of sub-mm surveys that demonstrate how the rest-frame FIR–sub-mm SEDs (250–500 μm) of galaxies can be used to measure their photometric redshifts with a conservative 1σ accuracy of $\Delta z \sim \pm 0.6$ over the redshift range $1 < z < 6$. Thus we can finally break the current *redshift deadlock* that limits our understanding of the evolution of the sub-mm galaxy population. From such precision in the individual galaxy redshifts, we can determine the star formation history for luminous sub-mm galaxies brighter than 3×10^{12} $L_\odot$ with an accuracy of ∼20 per cent. We consider the specific example of future surveys from BLAST. Furthermore we illustrate

© Royal Astronomical Society • Provided by the NASA Astrophysics Data System

2002MNRAS.335..871H

Table 1. Examples of the number of detected galaxies and their redshift distributions in alternative 50-h 250 μm BLAST surveys to be undertaken during a series of future long-duration (∼10–15 d) balloon flights.

Survey area (deg^2)	1σ depth	No. of pixels	No. of detected galaxies $>5\sigma$	$>10\sigma$	No. of $>5\sigma$ galaxies $z>1$	$z>3$
1.0	5 mJy	18334	835	265	765	147
2.0	7 mJy	36668	1012	291	927	151
4.0	10 mJy	73336	1100	294	988	147
9.0	15 mJy	165006	1111	247	1023	129
36.0	30 mJy	660024	990	246	895	105

how these estimates can be improved with sub-mm observations using the more sensitive SPIRE camera on the *Herschel* satellite, and additionally with the inclusion of longer-wavelength ground-based 850-μm data from SCUBA. In Paper II of this series (Aretxaga et al. 2002) we develop this photometric-redshift estimation technique, and apply it to the existing multifrequency data for the population of ∼140 sub-mm galaxies detected in SCUBA and MAMBO surveys. We include, for the first time, an appropriate treatment of the observational errors at sub-mm to radio wavelengths, and provide an accurate measurement of the redshift distribution for sub-mm galaxies.

The following cosmological model is adopted throughout the paper: $\Omega_\Lambda = 0.7$, $\Omega_M = 0.3$, $H_0 = 67\,\mathrm{km\,s^{-1}\,Mpc^{-1}}$.

2 PHOTOMETRIC REDSHIFTS FROM WIDE-AREA SUBMILLIMETRE SURVEYS

2.1 Designing the sub-mm surveys

To assess the accuracy of the photometric redshifts that can be determined from rest-frame FIR–sub-mm data, we generate mock catalogues of sub-mm galaxies from Monte Carlo simulations that mimic realistic observing data (Section 2.2). Thus, we must first have prior knowledge of the areas and sensitivities of the sub-mm surveys that will be conducted with BLAST, SPIRE, or any other existing or future sub-mm experiment, in order to achieve the scientific goals. We have simulated realistic surveys to satisfy this requirement. These simulations, which include an evolving population of sub-mm galaxies that are consistent with the observed number-counts (Fig. 1), and a foreground Galactic cirrus component, are described in more detail elsewhere (Hughes & Gaztañaga 2000; Gaztañaga & Hughes 2001; Chapin et al. 2001). In particular these simulations help us to understand how the analysis of the experimental survey data can be affected by telescope resolution, extragalactic and Galactic source confusion, survey sensitivity and noise, and sampling variances owing to clustering and shot-noise.

Provided the BLAST surveys are conducted towards regions of low Galactic cirrus ($I_{100\,\mu\mathrm{m}} < 1.4$ mJy sr^{-1}), then the BLAST survey confusion limit will be dominated by extragalactic sources. In the absence of any foreground cirrus, the simulation indicates that the extragalactic 3σ confusion limit of BLAST at 250–500 μm will be ∼20–30 mJy. For comparison the traditional estimate of extragalactic confusion, 1 source/30 beams (Condon 1974), suggests that confusion will begin to dominate below 30 mJy.

Hence, during a single long-duration balloon flight, BLAST will conduct a series of simultaneous large-area surveys (∼0.5–40 deg^2)

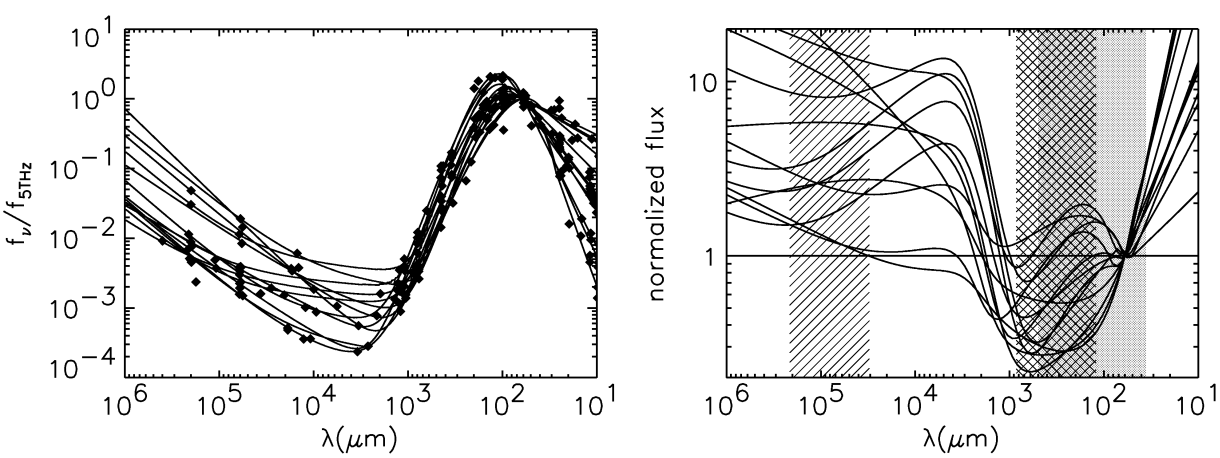

Figure 2. Left panel: rest-frame spectral energy distributions (SEDs) of 13 starburst galaxies, ULIRGs and AGN, normalized at 60 μm. Lines represent the best-fitting SED models to the data (diamonds) and include contributions from non-thermal synchrotron emission, free–free and greybody thermal emission. The parameters that describe the composite model for each galaxy, previously unpublished SED data and references for the remaining SED data are given in Chapin et al. (in preparation). Right panel: composite SED models for the identical 13 template galaxies shown in the left panel, normalized at 60 μm and scaled to the flux density of Arp220 at each wavelength. The vertically bounded regions (slanted, crossed and shaded) correspond to the rest-frame wavelength regimes covered by observations at 1.4 GHz, 850 μm and in the BLAST filters (500–250 μm) respectively for galaxies at $z = 0$–6. This representation of the SEDs shows more clearly the wavelength regimes in which the minimum dispersion in galaxy colours can be expected. Hence photometric redshifts determined from flux ratios between ∼100–1000 μm are the most independent of assumptions regarding the SED of the sub-mm galaxy.

© Royal Astronomical Society • Provided by the NASA Astrophysics Data System

2002MNRAS.335..871H

at 250, 350 and 500 μm, down to a 1σ sensitivity of 5 mJy, detecting in each survey ~1000 luminous sub-mm galaxies ($>10^{12}$ $L_\odot$) between $0.5 < z < 6$ (Table 1). The accuracy with which photometric redshifts can be determined from surveys of this magnitude is discussed in the following sections.

2.2 Monte Carlo simulations of sub-mm galaxy colours

Measurements of photometric redshifts determined from FIR–sub-mm–radio data usually do not include a rigorous analysis of the errors and the uncertainties in the calculations (Hughes et al. 1998; Blain 1999; Carilli & Yun 1999, 2000; Dunne et al. 2000; Eales et al. 2000; Barger et al. 2000). The desire to assign a degree of confidence (probability) to the photometric redshift of any individual sub-mm galaxy motivated the development of the Monte Carlo simulations, taking into account the imprecise knowledge of the luminosity function of sub-mm galaxies, the dispersion in the luminosity-dependent SEDs, absolute calibration and observational photometric errors (Aretxaga et al. 2001, 2002). From these individual redshifts it is then possible to provide a robust statistical measure of the redshift distribution for the entire sub-mm population.

In the case of BLAST (and also SPIRE), the power of this simple technique to derive redshifts arises from the unique ability of these experiments to conduct observations at 250–500 μm that bracket the ubiquitous rest-frame FIR peak (at ~60–150 μm) in the SEDs of high-redshift ($1 \leqslant z \leqslant 4$) galaxies undergoing a significant amount of star formation.

The adopted recipe that generates mock catalogues of galaxies between $z = 0$ and $z \sim 6$, for a given wavelength and under the chosen cosmological model, is summarized below.

(i) Use a single representative SED to calculate the distribution of rest-frame FIR luminosities of galaxies, at all redshifts, from an evolving 60 μm local luminosity function, $\phi[L, 0]$ (Saunders et al. 1990), that reproduces the observed sub-mm number counts. We adopt a model of pure luminosity evolution, $\phi[L, z] = \phi[L/L^*(z)]$, where

$$L^*(z) = \begin{cases} (1+z)^{3.2} L^*(0) & \text{for} \quad z \leqslant 2 \\ 33.6 L^*(0) & \text{for} \quad 2 < z \leqslant 6 \end{cases} . \tag{1}$$

It has been verified that an alternative choice of SED can compensate for small differences in the evolutionary model, and hence still reproduce the source counts (Fig. 1).

(ii) Randomly assign an SED from a library of 13 template starburst galaxies, ULIRGs and AGN (Fig. 2) to each of the galaxies in the mock catalogue, and use this SED to calculate the intrinsic sub-mm colours. The most crucial assumption of the paper occurs at this point in the simulation. We assume no correlation between the shape of the SED and luminosity (or redshift), and instead rely on the assumption that our library of 13 template SEDs is representative of those that exist at high z. The library, which includes M82, NGC 1614, NGC 3227, NGC 2992, NGC 4151, NGC 7469, NGC 7771, IZw1, Mkn231, Mkn273, Arp220, IRAS10214 and the 'Cloverleaf' quasar (H1413+117), contains galaxies with FIR luminosities in the range of $\log L_{\rm FIR}/L_\odot = 9.6$–$12.3$. The sample includes a mixture of AGN and starburst galaxies, and composite galaxies with both an AGN and a luminous extended FIR starburst region. The dust temperature (~30–60 K) and emissivity index ($\beta = 1.4 \pm 0.3$), which define the shape of their rest-frame FIR–sub-mm spectra are independent of the type or strength of nuclear activity. As mentioned in Section 1, the sensitivity of the sub-mm observations restricts the surveys to a detection threshold of $\log L_{\rm FIR}/L_\odot > 12$. Thus, an implicit assumption in this method is that one can simply scale the SED of a lower luminosity galaxy to represent that of a high-redshift sub-mm galaxy. Furthermore, there is no conclusive evidence that the rest-frame FIR–sub-mm SEDs of galaxies vary with luminosity, and redshift beyond the range of SEDs considered here – there is simply a lack of sufficient high signal-to-noise ratio observational data, over the appropriate wavelength regime, to come to any secure conclusions.

(iii) Add random noise (drawn from the distribution describing the measurement errors), and add a constant absolute flux calibration error to the intrinsic fluxes to allow a more realistic assessment of the photometric redshift accuracy: 1σ photometric errors of 5 and 2.5 mJy for the BLAST and Herschel/SPIRE observations respectively, and in both cases an absolute calibration error of 5 per cent. The combined simulated images of extragalactic sources and cirrus, described earlier in Section 2.1, determine the depth of the surveys considered here, ensuring that galaxy confusion dominates. However this Monte Carlo treatment of the photometric accuracy does not consider the contaminating effects of cirrus, clustering of galaxies, shot-noise or projection effects. These considerations are deferred to a future paper.

(iv) Finally, extract flux-limited catalogues from 1 deg^2 confusion-limited surveys at 250, 350 and 500 μm with $1\sigma = 5$ and 2.5 mJy sensitivities, appropriate for BLAST and SPIRE observations.

Fig. 3 shows an example of one of the possible combinations of sub-mm colours, for a catalogue of ~424 galaxies detected ($>3\sigma$) simultaneously at 250, 350 and 500 μm in a 1 deg^2 BLAST survey. As expected the dispersion in sub-mm colours is dominated by the observational errors and not by the differences between the shapes of the template SEDs. This is particularly true when the colour ratios are determined over a relatively small wavelength interval, as is the case for the 250, 350 and 500 μm observations. However, as we extend the wavelength baseline over which colours are calculated then the effect of differences in the galaxy SEDs on the photometric colours becomes increasingly significant (see Fig. 2). An example of this important effect can be found with the inclusion of longer wavelength data to the BLAST observations (Section 2.3.3), or perhaps more extreme, with the combination of 850-μm and 1.4-GHz fluxes (Carilli & Yun 2000) which are separated in wavelength by a factor >200. Thus, in general, without an adequate treatment of observational errors and a representative set of reference SEDs, photometric redshifts will be estimated with an over-optimistic accuracy.

2.3 Submillimetre photometric redshifts

Submillimetre photometric redshifts can be determined by calculating the probability that the the colours (including errors) of an observed sub-mm galaxy are consistent with the colours of every galaxy (with a known redshift) in the mock catalogue. The final redshift probability distribution, $P(z)$, of any galaxy is then simply the sum of the individual probabilities from the entire catalogue, or explicitly

$$P(z) = a \sum_{i,\forall z_i} \Phi(\boldsymbol{c}_i - \boldsymbol{c}_0), \tag{2}$$

where a is the normalization constant, such that $\int_0^{z_{\rm max}} P(z)\,{\rm d}z = 1$ where $z_{\rm max} = 6$. The multi-variate Gaussian probability distribution, Φ, for k colours, is given by

$$\Phi(\boldsymbol{c}_i - \boldsymbol{c}_0) = (2\pi)^{-k/2} |\mathbf{A}^{-1}|^{1/2} \exp\left(-\tfrac{1}{2}(\boldsymbol{c}_i - \boldsymbol{c}_0)' \mathbf{A}^{-1} (\boldsymbol{c}_i - \boldsymbol{c}_0)\right), \tag{3}$$

© Royal Astronomical Society • Provided by the NASA Astrophysics Data System

2002MNRAS.335..871H

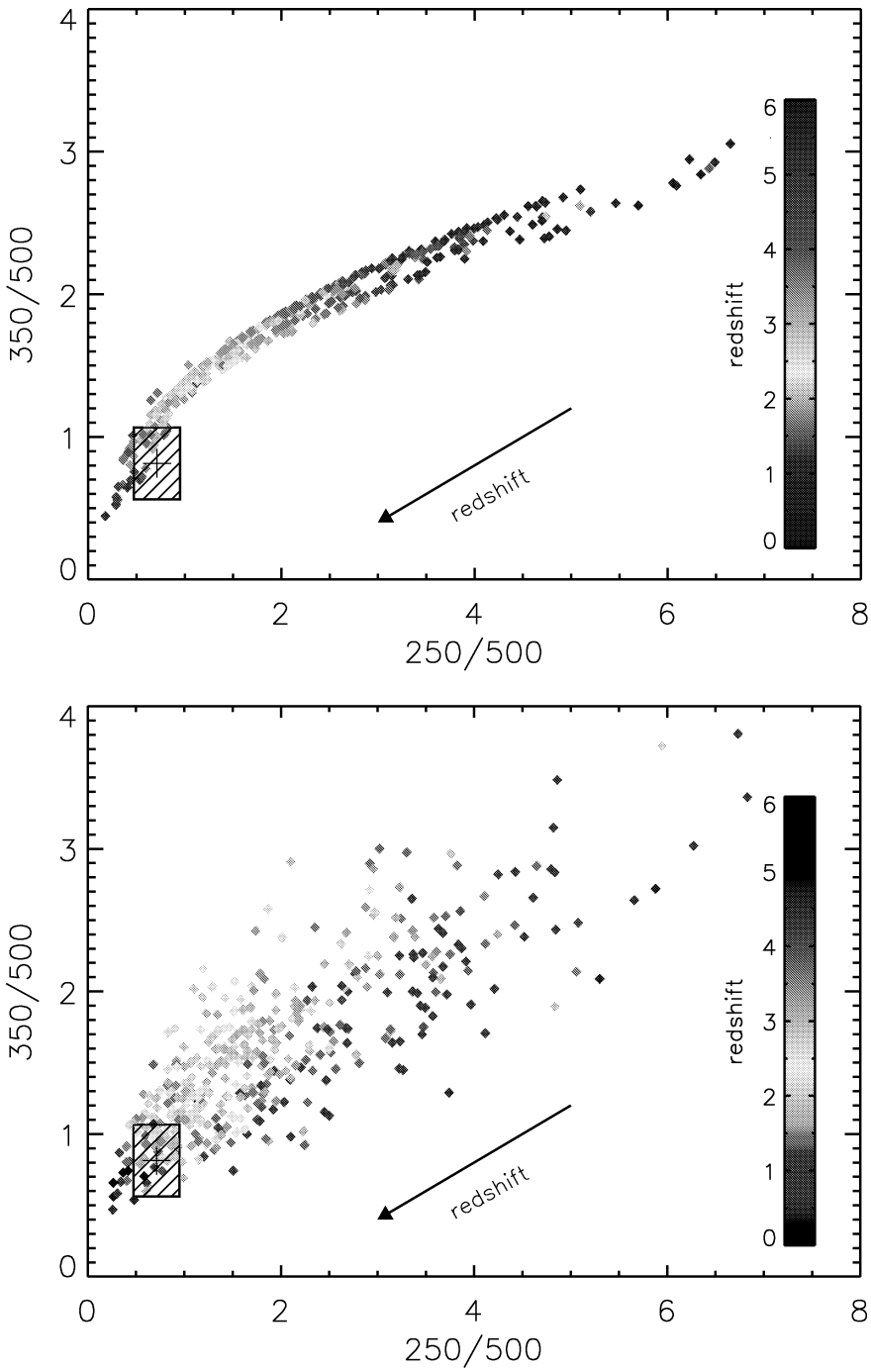

Figure 3. Colour–colour (350 μm/500 μm versus 250 μm/500 μm) versus redshift distribution for 424 galaxies detected ($>3\sigma$) simultaneously by BLAST in all 3 filters in a simulated 1-deg^2 survey. Top panel: colour distribution of detected galaxies without the inclusion of observational (photometric or calibration) errors. Bottom panel: colour distribution of detected galaxies with the inclusion of observational errors (5 per cent absolute calibration and a random measurement error drawn from a $1\sigma = 5$ mJy distribution), which dominate the scatter. The black cross marks the position of a 4×10^{12} $L_\odot$ galaxy at $z = 2.81$. The hashed rectangle represents the 1σ error on the measured colours. The redshift probability distribution for this galaxy is shown in Fig. 4.

where $\boldsymbol{c}_i$ is the colour vector of the ith mock galaxy, such that $z_i \in [z - \mathrm{d}z, z + \mathrm{d}z]$, and $\boldsymbol{c}_0$ is the colour vector of the test sub-mm galaxy, for which we want to derive its redshift distribution. **A** is the covariance matrix of the colour distribution, of elements

$$A_{\alpha\beta} = \langle(\bar{c}_\alpha - c_\alpha)(\bar{c}_\beta - c_\beta)\rangle, \quad (4)$$

for two colours α, β. In the majority of the analysis performed for this paper, the non-diagonal elements of the covariance matrix are small. When more than two colours are considered, for simplicity, the above prescription can be substituted with standard χ^2 statistics.

In this analysis, we have adopted redshift bins of width 0.5 ($\mathrm{d}z = 0.25$). The most probable redshift of the test sub-mm galaxy will

© Royal Astronomical Society • Provided by the NASA Astrophysics Data System

2002MNRAS.335..871H

be given by the mode of the discrete $P(z)$ distribution, estimated as the centroid of the Gaussian that best fits the 5 bins around the maximum of $P(z)$. The asymmetric error bars (z_-, z_+) correspond to 68 per cent confidence levels such that $\int_{z_-}^{z_+} P(z)\,\mathrm{d}z = 0.68$ and $(z_+ - z_-)$ is minimized.

2.3.1 *BLAST colours*

Fig. 4 shows two examples of the redshift distributions for sub-mm galaxies detected by BLAST at different levels of significance in all three filters. A further example of the broader distribution derived for a higher-z galaxy detected only at 500 μm is also shown in Fig. 4. The accuracy of the redshifts determined from BLAST data is described in more detail in Section 2.4, where we also compare the accuracy to those obtained from optical–IR colours and the 850 μm/1.4 GHz spectral index. The dispersion in the sub-mm photometric redshifts derived from three BLAST bands is $\Delta z = \pm 0.6$ averaged over all redshifts in the range $0 < z < 6$.

2.3.2 *SPIRE colours*

An increase in the sensitivity of the sub-mm observations (with SPIRE for instance) naturally translates into an increased accuracy of the redshift distributions. However the greater sensitivity of the SPIRE observations ($1\sigma = 2.5$ mJy) does not significantly improve the accuracy of the redshift distributions, compared with those determined from detections in all three BLAST filters. The redshift uncertainties for these sources are caused by a combination of the absolute calibration errors and the dispersion in the template SEDs. However SPIRE does provide a far greater redshift accuracy for the sources that BLAST detects in only one or two filters with low S/N (Fig. 5). Thus, if the advantage of the larger aperture of Herschel, the reduced confusion limit and higher sensitivity of SPIRE is to be realized, then a clearer understanding of the SEDs of high-z galaxies is first required.

2.3.3 *BLAST + 850-μm colours*

A greater improvement in the accuracy of the sub-mm photometric redshifts can be achieved by following-up BLAST (or SPIRE) surveys with longer-wavelength survey data (e.g. ground-based 850-μm SCUBA data), or vice versa. Fig. 6 shows the result of simulations that combine BLAST and 850-μm observations. The SCUBA data include a photometric measurement error of 2.5 mJy, to compare with the shallow UK 8-mJy SCUBA survey (Scott et al. 2002), and an absolute calibration error of 9 per cent. The addition of a longer-wavelength datum to the colour information has two advantages. First, the inclusion of one more colour simply assists the ability to constrain the redshift. This is particularly important for galaxies detected only at 500 and/or 350 μm (40 per cent of the sources in the BLAST surveys), which lie at the highest redshifts. Secondly, at $z > 4$ the BLAST filters all begin to sample the short-wavelength (rest-frame mid-IR) side of the FIR peak. This 850-μm extension to the BLAST wavelength coverage (250–500 μm) ensures that there is still a long-wavelength datum that brackets the rest-frame FIR peak (at least until $z \sim 7$). A clear illustration of these benefits is shown in Fig. 7 where high-z galaxies at $z > 4$, which had previously been confused with lower-z galaxies at $z = 2$–3 (using only data at 250–500 μm), are now symmetrically distributed about the $z = z_{\rm phot}$ regression line over the entire range $0 < z < 6$, with an improved average error of $\Delta z \sim \pm 0.4$. This correction applies only to a small fraction (4 per cent) of the galaxies detected in all three BLAST bands. This sub-mm method therefore continues to

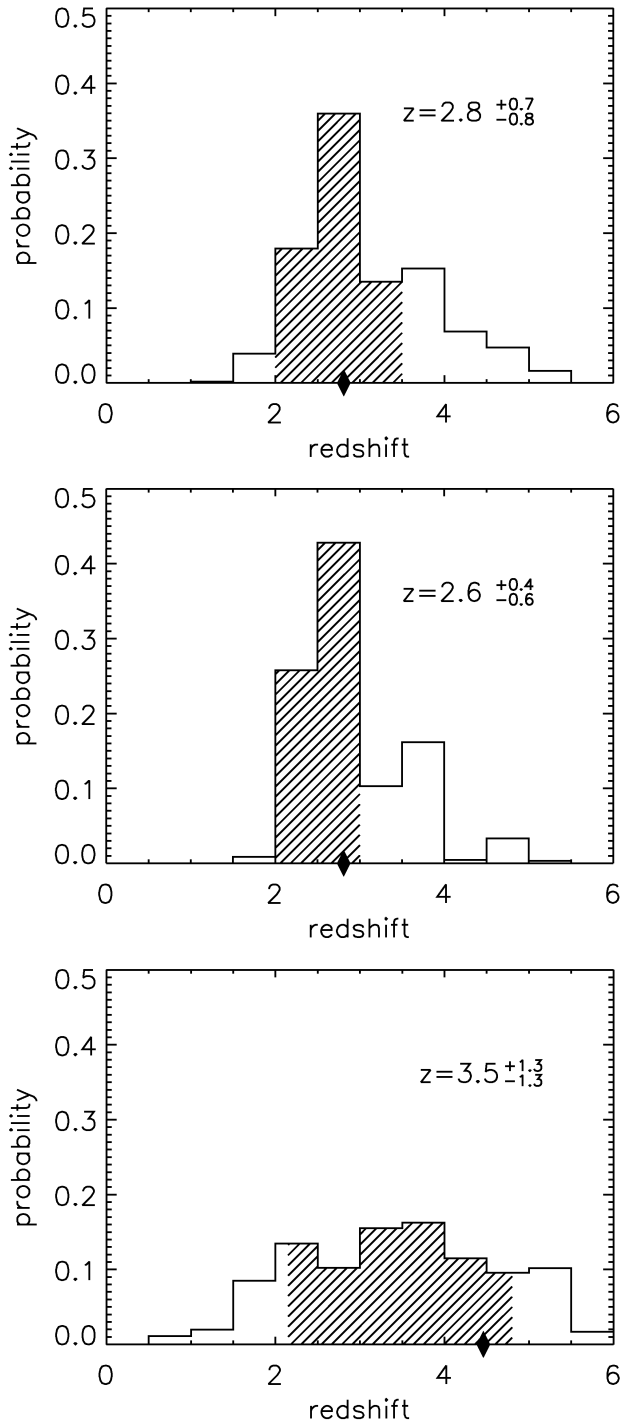

Figure 4. Redshift probability distributions for a selection of galaxies detected by BLAST. In all panels the diamonds mark the true redshifts of the galaxies. The photometric redshifts (modes and 68 per cent confidence intervals) are indicated in the labels and represented as the shaded areas of the histograms. Top panel: 4×10^{12} $L_\odot$ galaxy at $z = 2.81$, detected at 250 μm (19 mJy), 350 μm (21 mJy) and 500 μm (26 mJy), slightly below the BLAST survey confusion limit. The colours of this galaxy are represented as a cross in Fig. 3. Middle panel: 6×10^{12} $L_\odot$ galaxy at $z = 2.81$, detected at 250 μm (34 mJy), 350 μm (56 mJy) and 500 μm (45 mJy) with high S/N, above the BLAST survey confusion limit. Bottom panel: 4×10^{12} $L_\odot$ galaxy at $z = 4.46$, detected only at 500 μm (22 mJy).

© Royal Astronomical Society • Provided by the NASA Astrophysics Data System

2002MNRAS.335..871H

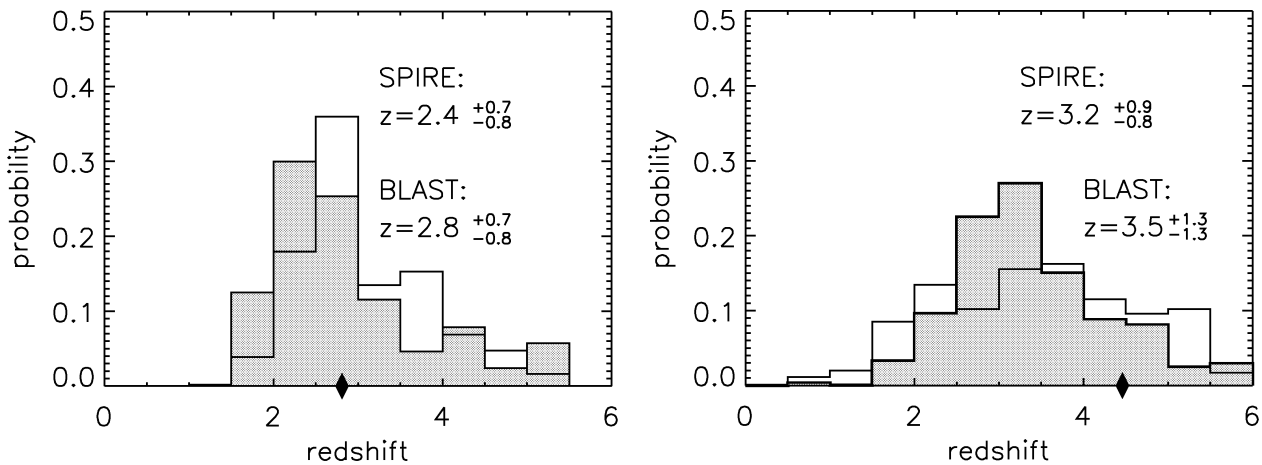

Figure 5. A comparison of the redshift probability distributions for two galaxies observed in a SPIRE survey, and a shallower BLAST survey (previously discussed in Fig. 4). Symbols and labels are the same as in Fig. 4. Left panel: 4×10^{12} $L_{\odot}$ galaxy at $z = 2.81$ detected simultaneously with three SPIRE filters (shaded histogram), compared with the BLAST redshift distribution (open histogram). Right panel: 4×10^{12} $L_{\odot}$ galaxy at $z = 4.46$ detected simultaneously in two SPIRE filters; at 350 μm (11 mJy) and 500 μm (20 mJy), compared with the distribution obtained from a single filter (500 μm) detection with BLAST.

provide unbiased estimates of photometric redshifts for the most distant galaxies.

Given this benefit of including longer-wavelength data, the deepest BLAST surveys will be selected to overlap the largest (0.5–1.0 deg^2) surveys carried out by the JCMT at 850 μm and IRAM at 1.25 mm. The extended wavelength coverage (250 μm–1.1 mm) will provide accurate redshift constraints out $z \sim 8$.

The analysis described in this paper simultaneously makes use of all of the available multifrequency data (unlike the simple one–colour versus redshift treatments described elsewhere), and takes into account the measurement errors and uncertainties in the SEDs of the template galaxies used to extrapolate the rest-frame luminosities of the sub-mm galaxies from their observed data.

2.4 Comparison of optical–IR, sub-mm and sub-mm–radio photometric redshifts

The photometric redshifts of galaxies derived from sub-mm BLAST data (250, 350 and 500 μm), using the method described above, are compared with the true redshifts in our mock catalogues. We have demonstrated that an average accuracy of $\Delta z(\mathrm{submm}) \sim 0.6$ can be achieved over the range $0 < z < 6$, although, as Table 2 shows, the scatter increases significantly for $z > 3.5$ for the reasons described in §2.3. The photometric redshifts measured from the optical-IR SEDs of galaxies in the *Hubble Deep Field* (HDF) (Fernández-Soto, Lanzetta & Yahil 1999; Rowan-Robinson 2001) have an accuracy that varies between $\Delta z(\mathrm{opt}) \sim 0.1$–0.6 over the same redshift range. However we note that the optical galaxies described in this HDF analysis are obviously not drawn from the same population as the sub-mm galaxies. The accuracy of the optical photometric redshifts must be much poorer if the technique is applied to the optically obscured SCUBA galaxies. The inclusion of longer wavelength data (e.g. 850 μm) to the BLAST data improves the photometric redshift accuracy to $\Delta z(\mathrm{submm}) \sim 0.4$, and extends the redshift range over which we can measure reliable redshifts to $0 < z < 6$ (Fig. 8 and Table 2). This means that, despite the greater wealth of data describing the optical–IR SEDs of galaxies and the number of available optical–IR bands, the sub-mm photometric redshifts of the sub-mm galaxy population can be determined with a similar accuracy to the optical-IR photometric redshifts of optically selected galaxies at $z > 1.5$ (Fig. 8).

We also draw attention to the lowest-redshift bin, $0.5 < z < 1.5$, in Table 2, which shows that the addition of 850-μm data decreases the redshift accuracy, compared to that derived from the shorter wavelength 250–500 μm observations. This is a result of the fact that the brightness of low-redshift galaxies, assuming our evolutionary model for the luminosity function, will necessarily have low S/N detections in an 850-μm survey with a 1σ sensitivity of 2.5 mJy. Thus the low S/N 850-μm detections, when combined with the BLAST data, allows a greater range of redshifts to be consistent with the observed colours. Conversely the addition of shorter wavelength Space Infrared Telescope Facility (SIRTF) data with high S/N will improve the accuracy of our photometric redshift estimates at $z < 1.5$.

The redshift accuracies determined from BLAST and BLAST+850-μm data (columns 3 and 4 in Table 2) are compared with those obtained from the identical data in our mock catalogues using the 350-GHz (850-μm) to 1.4-GHz spectral index ($\alpha_{1.4}^{350}$) described by Carilli & Yun (2000). The simulations include a photometric error of 7 μJy, and absolute calibration error of 3 per cent to compare with the deepest VLA surveys. As Fig. 8 clearly illustrates, the photometric redshifts obtained with the sub-mm/radio method suffer a large scatter ($\Delta z(\alpha_{1.4}^{350}) > 1.5$), particularly at $z > 2$, where small differences in $\alpha_{1.4}^{350}$ result in large differences in the redshift estimates. The inability of the 850–1.4-GHz index to determine accurate redshifts at $z > 2$ has already been noted by Carilli & Yun (2000). At $z < 2.5$, photometric redshifts using $\alpha_{1.4}^{350}$ are still less accurate than those determined from the sub-mm (250–850 μm) method described in this paper. This is due, in part, to the larger scatter of the SEDs at radio wavelengths (Fig. 2). Naturally, any redshift estimated from a single colour index (e.g. $\alpha_{1.4}^{350}$) is also, in general, going to a offer a less stringent constraint than the use of two or more colours.

2.5 Measuring the star formation history from sub-mm surveys

The measurement of redshift probability distributions for a large sample of sub-mm galaxies provides the information necessary to derive robust estimates of global properties of the population, such as the SFR history, even if the redshift and luminosity of individual galaxies are not known with a great degree of precision. The

© Royal Astronomical Society • Provided by the NASA Astrophysics Data System

2002MNRAS.335..871H

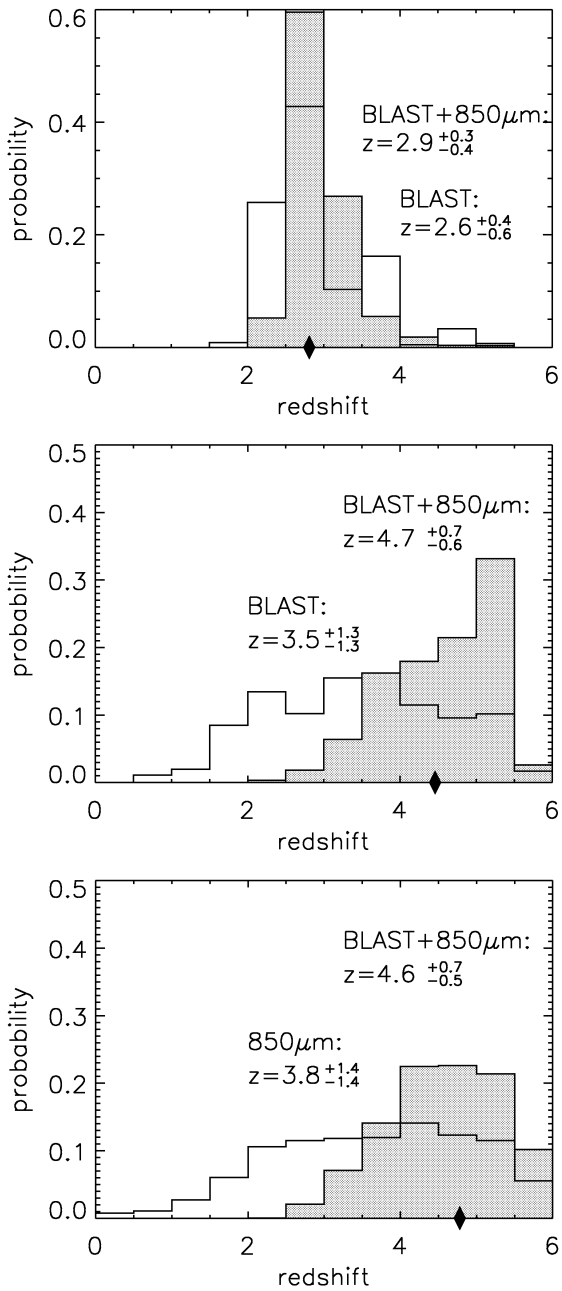

Figure 6. Redshift probability distributions demonstrating the advantages of follow-up observations that extend the sub-mm wavelength coverage. Symbols and labels are the same as in Fig. 4. Top panel: 6×10^{12} $L_\odot$ galaxy at $z = 2.81$ detected by BLAST in all 3 filters (open histogram), previously discussed in Fig. 4. The redshift estimate improves with follow-up observations at longer wavelengths. The shaded histogram illustrates the benefit of detecting the same galaxy at 850 μm (8 mJy) in a shallow sub-mm survey ($\sigma_{850\,\mu m} = 2.5$ mJy), e.g. similar to the UK 8-mJy SCUBA survey (Scott et al. 2002). Middle panel: this example shows the 4×10^{12} $L_\odot$ galaxy at $z = 4.46$, initially detected by BLAST in only one filter (500 μm), previously discussed in Fig. 4 (open histogram). Again, the detection at 850 μm (16 mJy) is sufficiently discriminating to constrain the distribution to higher redshifts (shaded histogram). Bottom panel: 5×10^{12} $L_\odot$ galaxy at $z = 4.78$ detected at 850 μm (8 mJy) in a shallow SCUBA survey (open histogram). Despite the non-detection of this galaxy by BLAST, in all three filters (250, 350, 500 μm), these shorter wavelength data can place an improved constraint on the redshift distribution (shaded histogram).

photometric redshift distribution of an individual galaxy allows the determination of its probable contribution to the total FIR luminosity density in a given redshift interval.

This calculation is performed via 100 Monte Carlo samples drawn from the redshift probability distribution for each galaxy in the mock survey. The FIR luminosities of these galaxies are then derived from the fluxes in the mock catalogue and the new synthetic redshifts. The SED from the template library that best represents the colours (including observational errors) of the whole population is used to calculate the necessary k correction. This SED will in general be different from that assigned in the original catalogue. We then calculate the uncertainty in the k correction, and therefore the error in the FIR luminosity, by randomly selecting any SED in the template library. Thus we remove any bias introduced into the reconstruction of the SFR through the choice of a single SED intended to represent the whole population of sub-mm galaxies. Finally, the star formation density is calculated from the mean of the Monte Carlo FIR luminosities, assuming $\mathrm{SFR/M_\odot\ yr^{-1}} = 2.0 \times 10^{-10}\ L_{\mathrm{FIR}}/\mathrm{L_\odot}$ (Hughes, Dunlop & Rawlings 1997).

A deep BLAST survey, combined with a wide-area shallow SCUBA survey ($S_{850\,\mu m} > 8$ mJy), can recover the SFR density arising from galaxies with $L_{\mathrm{FIR}} \geqslant 3 \times 10^{12}$ $\mathrm{L_\odot}$ at $0.5 \leqslant z \leqslant 5.5$ with an accuracy of ~20 per cent (Fig. 9). The completeness of the survey is ~98 per cent above 3×10^{12} $\mathrm{L_\odot}$ (Fig. 9). The SFR density derived from the mock combined BLAST and SCUBA survey is consistent with the preliminary results from the UK 8-mJy SCUBA survey (Scott et al. 2002), and provides a good illustration of the advantage of being able to derive photometric redshifts for the entire survey sample over a large redshift range.

3 CONCLUSIONS

Monte Carlo simulations of multiwavelength (250–850 μm) sub-mm surveys show that the majority of the scatter in the derived sub-mm colours will be due, in approximately equal parts, to the dispersion in the SEDs of galaxies in a library of templates, and the observational and calibration errors. Since we can control to some extent the quality of the experimental data, it is still the uncertainty in the observed (or model) SEDs of high-z starburst galaxies that will ultimately limit the accuracy of these photometric redshift predictions. Theoretical SEDs, based on radiative transfer models for high-z starburst galaxies (Efstathiou, Rowan-Robinson & Siebenmorgen 2000), can help in principle. However the low S/N, and restricted wavelength coverage of the available observational data for high-z starburst galaxies are consistent with such a broad range of theoretical models that they currently provide little discriminatory power in determining the most appropriate SEDs to use as templates. Consequently, one of the most straight-forward achievements of BLAST, but no less important, will be simply to provide an accurate empirical model of the temperature-sensitive SEDs for thousands of high-z galaxies at these critical short sub-mm wavelengths (250–500 μm).

The product of the simulations of sub-mm surveys described in this paper is the ability to calculate the probability distribution for the redshift of any individual galaxy, taking into account observational errors and the uncertainty in the appropriate template SED, without the requirement to first identify the optical, IR or radio counterpart. These simulations demonstrate that the combination of balloon-borne (airborne or satellite) short-wavelength sub-mm data at 250–500 μm, and longer-wavelength ground-based 850-μm data, for a statistical sample of galaxies can provide the rest-frame FIR

© Royal Astronomical Society • Provided by the NASA Astrophysics Data System

2002MNRAS.335..871H

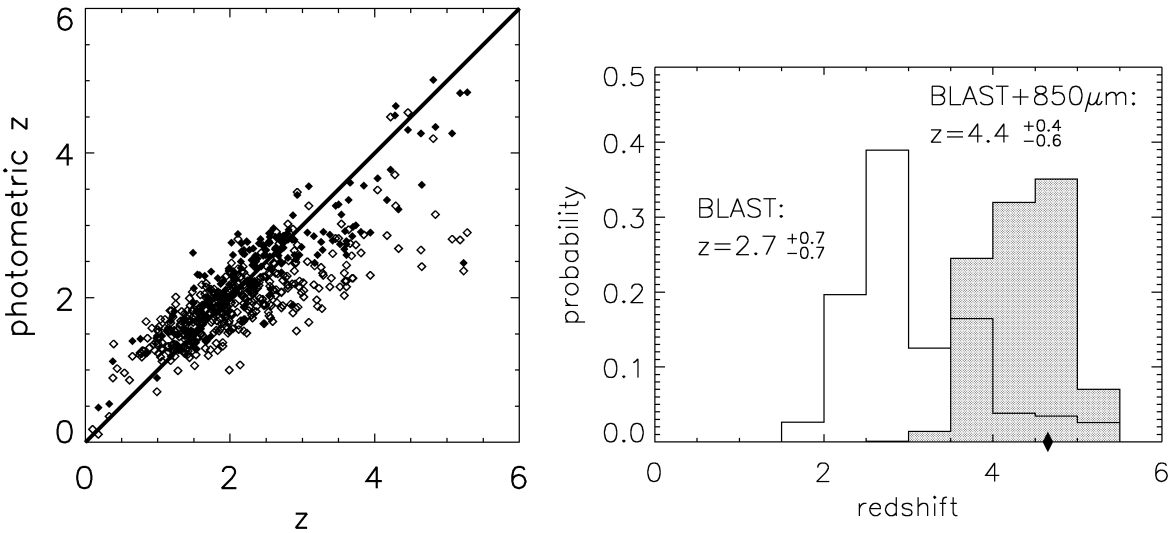

Figure 7. Left panel: photometric redshift versus true redshift relationship for 424 mock galaxies simultaneously detected at 250, 350 and 500 μm with BLAST in a 1 deg^2 survey. Open symbols show the relationship inferred using only BLAST data to derive the redshifts. Filled symbols show the relationships when the redshifts are estimated using colours based on BLAST and complementary 850-μm detections from a ground-based survey. The addition of 850-μm measurements significantly increases the accuracy at $z \geqslant 4$ since, at these redshifts, BLAST filters sample the rest-frame mid-IR to FIR (∼35–100 μm). The longer wavelength data bracket the rest-frame FIR peak of the highest-z objects, which enhances the diagnostic power for the photometric technique discussed in this paper. Right panel: example of the correction obtained for galaxies at $z > 4$ when 850-μm observations are included in the photometric redshift analysis. The redshift distributions for a 1×10^{13} L$_\odot$ galaxy at $z = 4.65$ with detections at 250 μm (18 mJy), 350 μm (29 mJy), 500 μm (27 mJy) and 850 μm (20 mJy) are shown as open (BLAST detections only) and shaded (BLAST and 850-μm detections) histograms. This correction, whilst significant, only applies to 4 per cent of the entire sample detected in three bands.

luminosity distribution, and hence the star formation history of the entire sub-mm population.

The precision of redshift estimates determined from short-wavelength sub-mm observations (250–500 μm) is encouraging, with a 1σ dispersion of Δz(submm) = 0.4–0.6 (depending on the availability of longer-wavelength ground-based data, $\lambda \geqslant 850$ μm) over the range $0 < z < 6$. This sub-mm precision is comparable to the accuracy of the optical-IR photometric estimates of redshift, Δz(opt) ∼ 0.5 at $z > 2$, and significantly better than those provided by the 850-μm/1.4 GHz spectral index. An important consequence of these sub-mm redshift constraints is the ability to measure the star formation of luminous sub-mm galaxies ($L_{\rm FIR} > 3 \times 10^{12}$ L$_\odot$) with an unprecedented error of ∼20 per cent.

The advantage of having a constrained redshift probability distribution for individual sub-mm galaxies, without optical, IR or radio (continuum) counterparts, is that we can now determine the likelihood that a redshifted rotational CO transition-line falls into the frequency range of any particular spectral-line receiver on the next generation of large mm–cm telescopes (e.g. 100-m GBT, 50-m LMT). The opportunities to conduct mm-wavelength spectroscopic follow-up observations that will provide definitive molecular-line redshifts, and dynamical-mass estimates of sub-mm galaxies, are discussed further in Paper II (Aretxaga et al. 2002).

The combination of short-wavelength sub-mm data from BLAST, SPIRE or other facilities, and large single-dish millimetre wavelength telescopes provides a powerful combination to break the *redshift deadlock* that hinders our ability to understand the evolution and nature of the sub-mm starburst galaxy population.

Table 2. Comparison of the 1σ redshift accuracy, Δz, determined from a simulated survey with rms sensitivities of 5 mJy at 250, 350 and 500 μm, 2.5 mJy at 850 μm and 7 μJy at 1.4 GHz using different photometric colours in redshift bins between $0.5 < z < 5.5$. Column 2 – optical data (Fernandez-Soto et al. 1999, and Rowan-Robinson 2001 in parentheses); column 3 – sub-mm data from BLAST at 250, 350 and 500 μm; column 4 – extended sub-mm data from BLAST and additional 850-μm observations; column 5 – sub-mm (850 μm, 350 GHz) and radio (1.4-GHz) data. Redshifts have been calculated from $\alpha_{1.4}^{350}$, defined as the spectral index between 350 and 1.4 GHz, using the formalism described by Carilli & Yun (2000). The redshifts in columns 3, 4 and 5 have been calculated for galaxies drawn from the same mock catalogue.

Redshift bin z	Optical + IR	Redshift accuracy Δz BLAST	BLAST + 850 μm	850 μm + 1.4 GHz
0.5–1.5	0.1 (0.2)	0.3	0.5	0.7
1.5–2.5	0.5 (0.3)	0.3	0.3	1.2
2.5–3.5	0.5 (0.4)	0.7	0.3	1.4
3.5–4.5	0.5 (0.2)	1.1	0.7	2.1
4.5–5.5	0.3 (0.6)	2.1	0.6	2.5

ACKNOWLEDGMENTS

We thank the anonymous referee for constructive suggestions to improve this paper. This work has been funded by CONACYT grants 32180-E and 32143-E. The development of BLAST is supported in part by NASA grant NAG5-92291. DHH, IA, and ELC thank Mark Devlin and the Physics & Astronomy Department at University of Pennsylvania, Philadelphia for their financial support and hospitality in 2001 June, during which part of this work was carried out.

REFERENCES

Aretxaga I., Hughes D. H., Chapin E., Gaztanaga E., 2001, in de Petris M., Gervasi M., eds, Experimental Cosmology at Millimetre Wavelengths. AIP Conf. Proc. Vol. 616. Am. Inst. Phys., New York, p. 354, in press (astro-ph/0111508)

© Royal Astronomical Society • Provided by the NASA Astrophysics Data System

2002MNRAS.335..871H

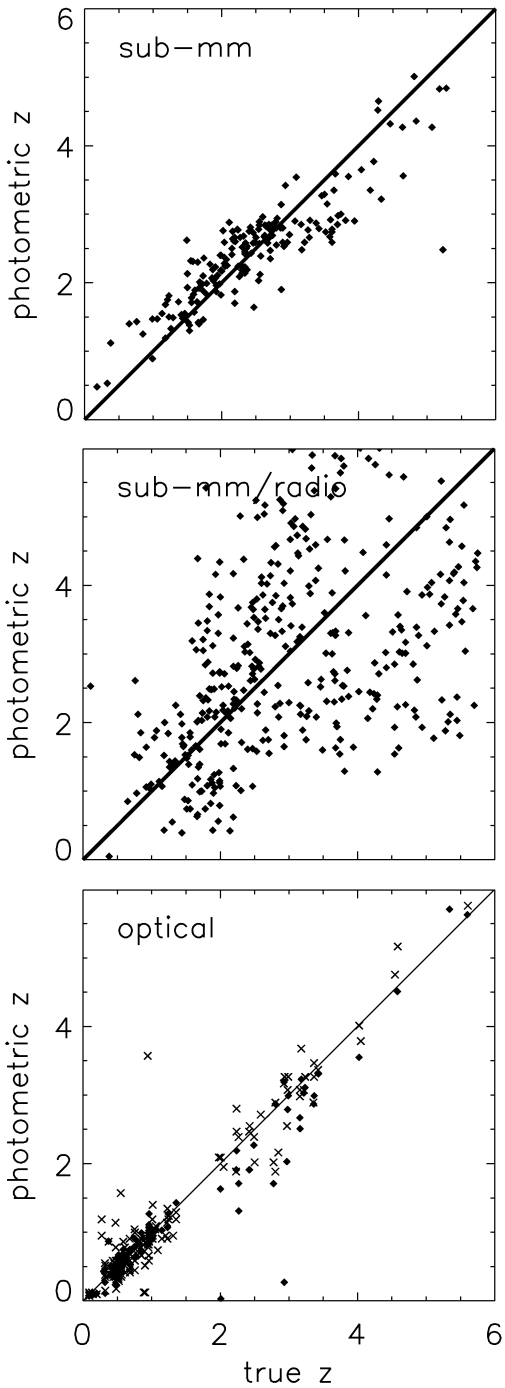

Figure 8. Top panel: Sub-mm photometric redshifts versus true redshifts for 189 mock galaxies simultaneously detected at 250, 350, 500 and 850 μm in 1 deg^2. The overall rms scatter in the sub-mm photometric redshifts, determined from the combined BLAST and SCUBA 850-μm data, is Δz(submm) ~ 0.4 in the redshift range $0 < z < 6$. Middle panel: sub-mm–radio photometric redshifts versus true redshifts for galaxies selected from the same catalogue as in the top panel, using $\alpha_{1.4}^{350}$, the 350–1.4 GHz spectral index described by Carilli & Yun (2000). Bottom panel: optical–IR photometric redshifts versus spectroscopic redshifts in the *Hubble Deep Field*–108 galaxies (Fernández-Soto et al. 1999 – diamonds) and 156 galaxies (Rowan-Robinson 2001–crosses). The optical–IR photometric redshifts, for galaxies at $z_{\rm true} \geqslant 2$, show a dispersion of Δz(opt) ~ 0.5 (excluding the outlying sources).

Aretxaga I., Hughes D. H., Chapin E., Gaztanaga E., Dunlop J. S., 2002, MNRAS, submitted (Paper II)

Barger A. J., Cowie L. L., Sanders D. B., Fulton E., Taniguichi Y., Sato Y., Kawara K., Okuda H., 1998, Nat, 394, 248

Barger A. J., Cowie L. L., Richards E. A., 2000, AJ, 119, 2092

Bertoldi F., Menten K. M., Kreysa E., Carilli C. L., Owen F., 2000, in Wilner D. J., ed., Highlights of Astronomy 12, Cold Gas and Dust at High Redshift, in press (astro-ph/0010553)

Blain A. W., 1999, MNRAS, 309, 955

Borys C., Chapman S. C., Halpern M., Scott D., 2002, MNRAS, 330, 63

Carilli C. L., Yun M. S., 1999, ApJ, 513, L13

Carilli C. L., Yun M. S., 2000, ApJ, 530, 618

Chapin E., Hughes D. H., Kelly B. D., Holland W. S., 2001, in de Petris M., Gervasi M., eds, Experimental Cosmology at Millimetre Wavelengths. AIP Conf. Proc. Vol. 616. Am. Inst. Phys., New York, p. 357

Chapman S. C. et al., 2000, MNRAS, 319, 318

Chapman S. C., Scott D., Borys C., Fahlman G. G., 2002, MNRAS, 330, 92

Condon J. J., 1974, ApJ, 188, 279

Devlin M. et al., 2001, in Lowenthal J., Hughes D. H., eds, Deep Millimetre Surveys: Implications for Galaxy Formation and Evolution. World Scientific, Singapore, p. 59

Downes D. et al., 1999, A&A, 347, 809

Dunlop J. S., 2001, in van Bemmel M., Wilkes B., Barthel P., eds, The FIR and Submillimeter Spectral Energy Distributions of Active and Starburst Galaxies, Elsevier New Astronomy Reviews Vol. 45. Elsevier, Amsterdam, p. 609

Dunne L., Clements D. L., Eales S. A., 2000, MNRAS, 319, 813

Eales S. A., Lilly S., Gear W., Dunne L., Bond J. R., Hammer F., Le Fèvre O., Crampton D., 1999, ApJ, 515, 518

Eales S. A., Lilly S., Webb T., Dunne L., Gear W., Clements D. L., Yun M., 2000, AJ, 120, 2244

Efstahiou A., Rowan-Robinson M., Siebenmorgen R., 2000, MNRAS, 313, 734

Fernández-Soto A., Lanzetta K., Yahil A., 1999, ApJ, 513, 34

Fixsen D. J., Dwek E., Mather J. C., Bennett C. L., Shafer R. A., 1998, ApJ, 508, 123

Fox M. J. et al., 2002, MNRAS, 331, 839

Frayer D. T., Ivison R. J., Scoville N. Z., Yun M., Evans M. S., Smail I., Blain A. W., Kneib J.-P., 1998, ApJ, 506, L7

Frayer D. T., Smail I., Ivison R. J., Scoville N. Z., 2000, AJ, 120, 1668

Gautier T. N., Boulanger F., Pérault M., Puget J. L., 1992, AJ, 103, 1313

Gaztañaga E., Hughes D. H., 2001, in Lowenthal J., Hughes D. H., eds, Deep Millimetre Surveys: Implications for Galaxy Formation and Evolution. World Scientific, Singapore, p. 131

Gear W. K., Lilly S. J., Stevens J. A., Clements D. L., Webb T. M., Eales S. A., Dunne L., 2000, MNRAS, 316, 51

Hauser M. G. et al., 1998, ApJ, 508, 25

Holland W. S. et al., 1999, MNRAS, 303, 659

Hughes D. H., 2000, in Mazure A., Le Févre O., Le Brun V., eds, ASP Conf. Set. Vol. 200, Clustering at High Redshift. Astron. Soc. Pac., San Francisco, p. 81

Hughes D. H., Gaztañaga E., 2000, in Favata F., Kass A., eds, Star formation from the Small to the Large Scale, ESA SP-445. ESA, Noordwijk, p. 29

Hughes D. H., Dunlop J. S., Rawlings S., 1997, MNRAS, 289, 766

Hughes D. H. et al., 1998, Nat, 394, 241

Ivison R. I., Smail I., Blain A., Kneib J-P., Frayer D., 1999, Ap&SS, 266, 285

Ivison R. J., Smail I., Barger A. J., Kneib J.-P., Blain A. W., Owen F. N., Kerr T. H., Cowie L. L., 2000, MNRAS, 315, 209

Kreysa E. et al., 1998, in Phillips T. G., ed., Proc. SPIE, Vol. 3357, 319

Lagache G., Puget J. L., 2000, A&A, 355, L17

Lilly S. J., Eales S. A., Gear W. K., Hammer F., Le Fèvre O., Crampton D., Bond J. R., Dunne L., 1999, ApJ, 518, 641

Lutz D. et al., 2001, A&A, 378, 70

Madau P., Ferguson H. C., Dickinson M. E., Giavalisco M., Steidel C. C., Fruchter A., 1996, MNRAS, 283, 1388

Peacock J. A. et al., 2000, MNRAS, 318, 535

© Royal Astronomical Society • Provided by the NASA Astrophysics Data System

2002MNRAS.335..871H

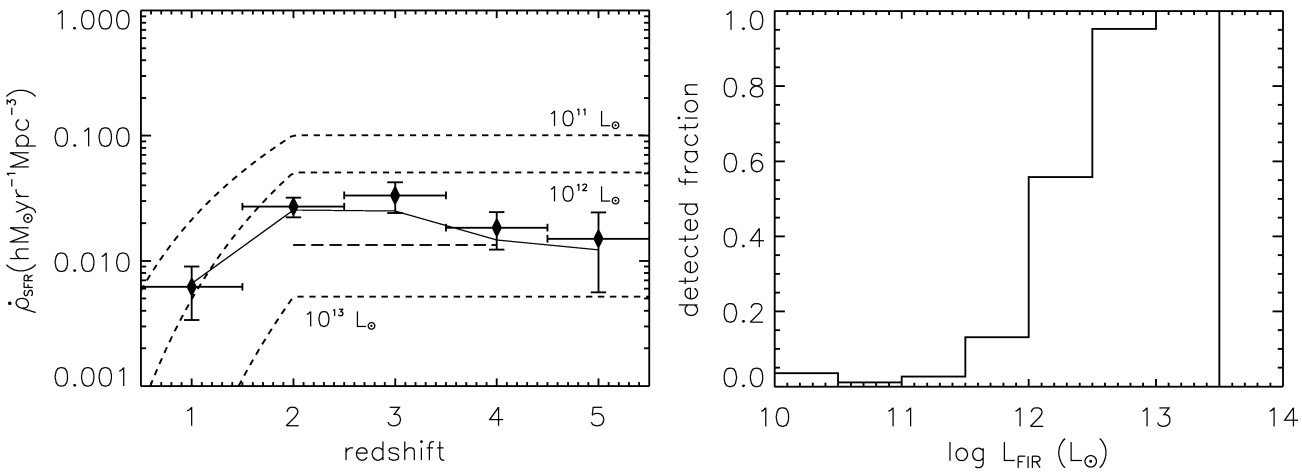

Figure 9. Left panel: global star formation rate history of galaxies detected in at least 2 filters from a combined BLAST ($3\sigma = 15$ mJy) and wide-area SCUBA 850-μm survey ($3\sigma = 8$ mJy). Filled diamonds represent the recovered values of the SFR using the photometric redshift distributions. We compare these values with the true SFR included in the mock catalogue (shown as a solid line) before measurement errors are introduced. The 3σ error bars of the reconstructed SFR are dominated by the uncertainty of the SED that should be used to derive the 60-μm luminosities of the mock galaxies (which have intrinsically different SEDs), and not by the accuracy of the redshift determinations. The long-dashed horizontal line shows an estimate of the minimum SFR density for sub-mm galaxies that have been detected in the UK 8-mJy SCUBA 850-μm survey (Scott et al. 2002), assuming that the SCUBA galaxies lie between $2 < z < 4$. The short-dashed curves represent the theoretical SFR arising from galaxies of FIR luminosities $>10^{11-13}$ L$_\odot$ derived from the evolutionary model adopted in the simulations Section 2.2. Right panel: fraction of galaxies, per luminosity interval, detected at all redshifts in the mock combined BLAST and wide-area SCUBA survey. The completeness of the survey is ~98 per cent for galaxies $>3\times10^{12}$ L$_\odot$.

Puget J.-L., Abergel A., Bernard J.-P., Boulanger F., Burton W. B., Désert F.-X., Hartmann D., 1996, A&A, 308, L5

Richards E. A., 1999, ApJ, 513, L9

Rowan-Robinson M., 2001, http://astro.ic.ac.uk/mrr/photz/photzapj.ps

Sanders D. B., Mirabel I. F., 1996, ARA&A, 34, 749

Saunders W., Rowan-Robinson M., Lawrence A., Efstathiou G., Kaiser N., Ellis R. S., Frenk C. S., 1990, MNRAS, 242, 318

Scott S. et al., 2002, MNRAS, 331, 817

Smail I., Ivison R. J., Blain A. W., 1997, ApJ, 490, L5

Smail I., Ivison R. J., Kneib J.-P., Cowie L. L., Blain A. W., Barger A. J., Owen F. N., Morrison G., 1999, MNRAS, 308, 1061

Smail I., Ivison R. J., Owen F. N., Blain A. W., Kneib J.-P., 2000, ApJ, 528, 612

Smail I., Ivison R. J., Blain A. W., Kneib J.-P., 2002, MNRAS, 331, 495

Steidel C. C., Giavalisco M., Pettini M., Dickinson M., Adelberger K. L., 1996, ApJ, 462, L17

This paper has been typeset from a TEX/LATEX file prepared by the author.

© Royal Astronomical Society • Provided by the NASA Astrophysics Data System